Available online at www.sciencedirect.com

jmr&t Journal of Materials Research and Technology

journal homepage: www.elsevier.com/locate/jmrt

Original Article

Effective grain size refinement of an Fe-24Ni-0.3C metastable austenitic steel by a modified two-step cold rolling and annealing process utilizing the deformation-induced martensitic transformation and its reverse transformation

Wenqi Mao [a,b], *Si Gao* [a,*], *Yu Bai* [a,c,d], *Myeong-heom Park* [a], *Akinobu Shibata* [a,c,e], *Nobuhiro Tsuji* [a,c]

[a] *Department of Materials Science and Engineering, Kyoto University, Sakyo-ku, Kyoto, Japan*
[b] *J-PARC Center, Japan Atomic Energy Agency, Ibaraki, Japan*
[c] *Elements Strategy Initiative for Structural Materials, Kyoto University, Sakyo-ku, Kyoto, Japan*
[d] *School of Materials Science and Engineering, Dalian University of Technology, Dalian, China*
[e] *Research Center for Structural Materials, National Institute for Materials Science (NIMS), 1-2-1, Sengen, Tsukuba 305-0047, Japan*

ARTICLE INFO

Article history:
Received 22 December 2021
Accepted 5 February 2022
Available online 12 February 2022

Keywords:
Ultrafine grain
Transformation cycling
Martensitic transformation
Reverse transformation
Tensile property

ABSTRACT

Metastable austenitic steels having ultrafine grained (UFG) microstructures can be fabricated by conventional cold rolling and annealing processes by utilizing the deformation-induced martensitic transformation during cold rolling and its reverse transformation to austenite upon annealing. However, such processes are not applicable when the austenite has high mechanical stability against deformation-induced martensitic transformation, since there is no sufficient amount of martensite formed during cold rolling. In the present study, a two-step cold rolling and annealing process was applied to an Fe-24Ni-0.3C metastable austenitic steel having high mechanical stability. Prior to the cold rolling, a repetitive subzero treatment and reverse annealing treatment were applied. Such a treatment dramatically decreased the mechanical stability of the austenite and greatly accelerated the formation of deformation-induced martensite during the following cold rolling processes. As a result, the grain refinement was significantly promoted, and a fully recrystallized specimen with a mean austenite grain size of 0.5 μm was successfully fabricated, which exhibited both high strength and high ductility.

* Corresponding author.
E-mail address: gao.si.8x@kyoto-u.ac.jp (S. Gao).

https://doi.org/10.1016/j.jmrt.2022.02.031

1. Introduction

Ultrafine grained (UFG) metallic materials usually exhibit quite high strength owing to the Hall-Petch effect but poor tensile ductility due to the lack of strain hardening capability at a high stress level [1]. However, substantial tensile ductility could still be maintained in some alloys that exhibit transformation-induced plasticity (TRIP) phenomenon even when the microstructures are refined to the UFG scale [2,3]. It has been revealed that the formation of the hard deformation-induced martensite during the deformation can increase the strain hardening rate and prevent necking, leading to high ductility [4,5]. Thus, creating UFG microstructures in TRIP alloys is one of the promising strategies to realize both high strength and high ductility in those alloys.

UFG microstructures can be fabricated by the SPD processes, such as high-pressure torsion (HPT) [6], accumulative roll bonding (ARB) [7,8], and equal-channel angular pressing (ECAP) [9]. However, the SPD processes are usually complicated and high-cost, and the sizes of specimens are quite limited. Besides the SPD processes, it has also been reported that UFG metastable austenitic steel can be fabricated by conventional rolling and annealing processes [10–12]. The principle is to utilize deformation-induced martensitic transformation during deformation. The formation of martensite variants with different orientations could effectively subdivide the original austenite grain. Moreover, the formed martensite plates provide high density of nucleation sites for reverse austenite formation in the subsequent annealing. Succeeded cases can be widely found in Fe-Cr-Ni ASSs such as 301 [3], 304L [13], 304 [14] and 316LN [15] as well as in Fe-Cr-Mn ASSs like 201 and 202 [16,17]. However, the feasibility of this method is based on a premise that a large amount of martensite could be introduced during deformation, i.e., the metastable austenite has low mechanical stability against deformation-induced martensitic transformation. When the austenitic steels have relatively high mechanical stability, such processes are not applicable.

Fe-Ni-C alloys are traditional model alloys for studying the martensitic transformation and corresponding TRIP effect in austenitic steels, and the stability of the austenite greatly varies depending on the nickel or carbon content [18]. Previous researches demonstrated that the austenite grain size of the Fe-24Ni-0.3C steel could not be refined down to submicrometer range unless using the SPD processes in which a huge amount of plastic strain was introduced [2,19,20]. Jafarian [2] showed that fully recrystallized fine-grained austenitic Fe-24Ni-0.3C was fabricated by 6-cycle of the ARB process with subsequent annealing and the smallest austenite grain size achieved was 2.5 μm. Chen et al. [19,20] performed HPT process followed by annealing on the Fe-24Ni-0.3C, and the smallest recrystallized austenite grain size was 0.42 μm. More recently, the present authors refined the grain size of Fe-24Ni-0.3C down to 1.3 μm by a conventional two-step cold-rolling and annealing processes [21]. However, microstructures with sub-micrometer grain size still have not been achieved in Fe-24Ni-0.3C by the cold-rolling and annealing processes, because the austenite has high mechanical stability and limited martensite was formed during the cold-rolling. In the present work, the two-step cold-rolling and annealing process was modified by applying a prior repetitive subzero quench followed by a short-time annealing process. It was revealed that such cyclic thermal treatment dramatically decreased the mechanical stability of the austenite in the Fe-24Ni-0.3C and enhanced the formation of deformation-induced martensite in the subsequent cold rolling, thereby facilitating an ultra-grain refinement in the processes. A fully recrystallized microstructure having an average grain size of 0.5 μm was achieved in the Fe-24Ni-0.3C, which exhibited very high yield strength and good tensile ductility.

2. Material and methods

An Fe-24Ni-0.3C (wt.%) alloy was used in the present study and its chemical composition is shown in Table 1. The as-received plate having 20 mm in thickness was austenitized at 700 °C for 10 min and used as the starting material. The fabrication process of the material is illustrated in Fig. 1. The starting material was firstly quenched into a liquid nitrogen bath to obtain thermal martensite and then annealed at 600 °C in a salt bath for 30 s to obtain austenite through reverse transformation (A_f temperature: 500 °C measured by dilatometry). Such a subzero quench followed by a short-time annealing treatment was referred to as one transformation cycling. Five cycles of such transformation cycling were applied to the starting material and then a typical two-step cold rolling and annealing process was conducted. In the first step, the material was cold-rolled to 10 mm in thickness corresponding to a 50% thickness reduction and then annealed at 600 °C for 30 s. After the first annealing, the sample was cold-rolled to 1 mm by 90% thickness reduction and annealed at 650 °C for 30 s, which refers to the second step.

The microstructural observation was carried out by field emission scanning electron microscopy (SEM) and electron backscatter diffraction (EBSD) measurement with a step size of 300 nm on the transverse section parallel to the rolling direction. The specimen for the microstructure observation was prepared carefully by mechanical polishing to avoid the formation of deformation-induced martensite, followed by electropolishing using a 5% perchloric acid +95% ethanol electrolyte at 20 V for 2 min at room temperature. X-ray diffraction (XRD) using Cu-Kα irradiation (wavelength 1.5406 Å) was performed on the section plane parallel to the surface of the specimens to evaluate the volume fraction of the deformation-induced martensite in the cold-rolled

Table 1 – Chemical composition of Fe-24Ni-0.3C steel (wt.%).

Ni	C	Si	Mn	S	P	0	N	Fe
24.09	0.3	0.01	0.07	<0.0005	<0 005	0.0008	0.0006	Bal.

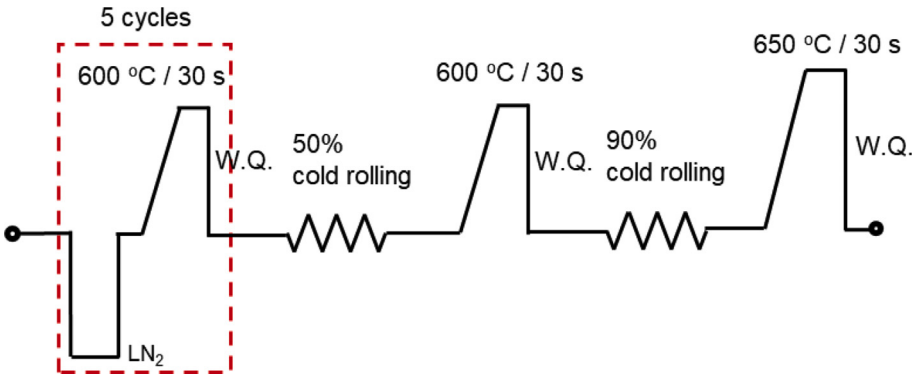

Fig. 1 – Schematic illustration of the modified two-step cold rolling and annealing process on the Fe-24Ni-0.3C austenitic steel.

specimen and the dislocation density of austenite in the specimen after the reverse annealing treatment. The volume fraction of martensite was evaluated from the integrated intensity of diffraction profile using the following equation [22],

$$f_{\alpha'} = \frac{\frac{1}{n}\sum_0^n I_{\alpha'}^{hkl} \Big/ R_{\alpha'}^{hkl}}{\frac{1}{n}\sum_0^n I_{\alpha'}^{hkl} \Big/ R_{\alpha'}^{hkl} + \frac{1}{n}\sum_0^n I_{\gamma}^{hkl} \Big/ R_{\gamma}^{hkl}} \quad (1)$$

where $I_{\alpha'}^{hkl}$ and I_{γ}^{hkl} are the integrated intensities of diffraction peaks $(hkl)_{\alpha'}$ and $(hkl)_{\gamma}$ of martensite and austenite, and $R_{\alpha'}^{hkl}$ and R_{γ}^{hkl} are the corresponding material scattering factors. In the present study, only the $(111)_{\gamma}$ and $(110)_{\alpha'}$ peaks were used to roughly estimate the volume fraction of martensite since the intensities of other diffraction peaks of austenite and martensite were too weak to be quantified precisely due to the strong fiber texture of the cold-rolled specimen. The dislocation density of the austenite after the reverse transformation was estimated by XRD using the classical Williamson-Hall method [23,24],

$$\frac{\omega \cos\theta}{\lambda} = \frac{0.9}{D} + \frac{2\varepsilon \sin\theta}{\lambda} \quad (2)$$

where ω is the full widths at half maximum (FWHM), θ is the angle of diffraction, λ is the X-ray wavelength, D is the crystallite size, and ε corresponds to the distortion related to the dislocation density. The dislocation density was estimated from the ε by the following equation

$$\rho = \frac{k\varepsilon^2}{b^2} \quad (3)$$

where b is the Burgers vector ($b = 0.253$ nm) and k is 16.1 for face-centered cubic metals [24].

The M_s temperature of the specimens was measured by differential scanning calorimeter (DSC) with a cooling rate of 1 °C/min. The hardness of specimens was determined using the Vickers hardness test by applying a 0.2 kg loading with a dwell time of 10 s. Tensile tests were performed at room temperature at an initial strain rate of 8.3×10^{-4} s^{-1}, using bone-shaped specimens with 10 mm gauge length, 2 mm gauge width, and 1 mm thickness. The tensile elongation was precisely measured by a digital image correlation method described in [25].

3. Results and discussion

The starting material was composed of fully austenitic structures having a mean grain size of around 40 μm, as shown in Fig. 2. By the first subzero treatment 80 vol% thermal martensite was formed in the material, as shown in Fig. 3(a). The IPF (Inverse pole figure) map of the martensite in the specimen shown in Fig. 3(b) revealed that the martensite

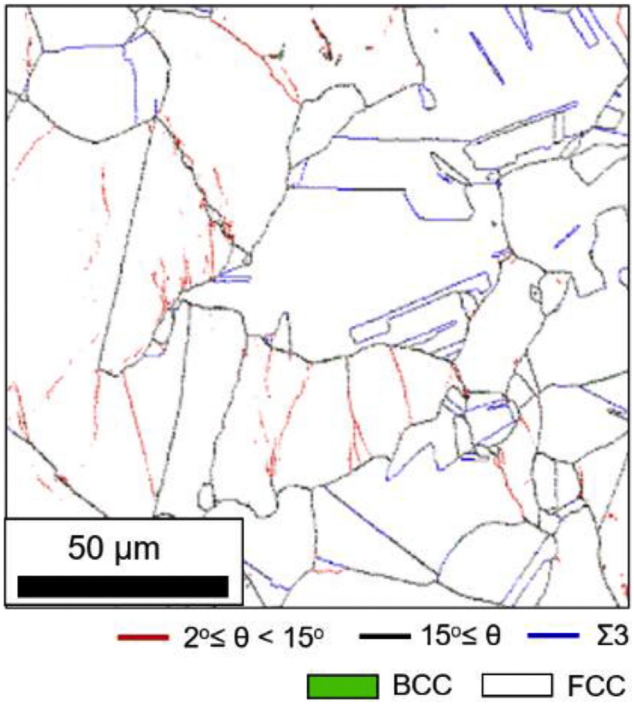

Fig. 2 – Grain boundary map superimposed with phase map of the starting material obtained by EBSD measurement. The low angle boundaries (LABG: $2^\circ \le \theta < 15^\circ$), high-angle grain boundaries (HAGB: $\theta \ge 15^\circ$), annealing twin boundaries (TB, Σ3) are respectively drawn in red, black, and blue lines. In the phase map, austenite and martensite are indicated by white and green, respectively.

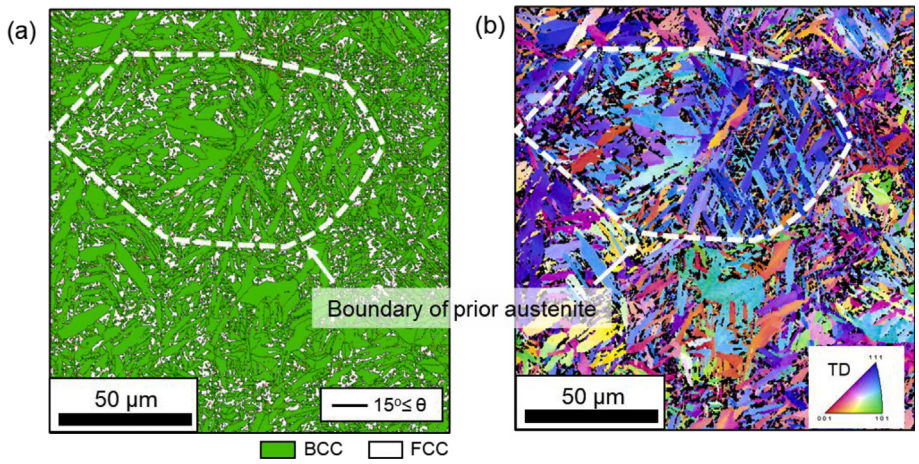

Fig. 3 – (a) Grain boundary map superimposed with phase map of the starting material after subzero-treatment at liquid nitrogen, and (b) Corresponding IPF map of the martensite. The grain boundary of one prior austenite grain was marked by the white dashed line, which was determined according to the orientation of the retained austenite.

blocks with different variants were formed within the marked prior austenite grain. Figure 4 shows the microstructures of the specimen after a complete transformation cycling. The specimen consisted of 100% austenite phase having equiaxed morphologies with a mean grain size of 40 μm which is almost the same as that of the starting material. In sharp contrast to the starting material, however, severe lattice distortions were noticed in the interior of reverse transformed austenite, which are manifested by the large number of low angle grain boundaries in Fig. 4(a) as well as by the gradient orientation distributions in the IPF map shown in Fig. 4(b). It has been known that the martensite to austenite reverse transformation in iron-based alloy takes place upon heating by two competing mechanisms: diffusional reversion and martensitic shear reversion. In diffusional reversion, the austenite grains nucleate and grow by a thermally activated atomic diffusion process, resulting in equiaxed austenite grains having low lattice distortion [26]. In contrast, martensitic shear reversion is a non-diffusional displacive transformation and the just reversed austenite grains contain a high density of dislocations that are generated during transformation to accommodate the transformation shear strain [26–28]. The microstructural features of the reversed austenite shown in Fig. 4 suggested that the reverse transformation took place via martensitic shear reversion, which was in line with the previous study of Aida et al. [29] by ex-situ observations in the same alloy.

The microstructural evolution of the specimen by transformation cycling was shown in Fig. 5. The phase map and grain boundary map in Fig. 5 (a)–(d) did not reveal a notable change in the morphology of reverse austenite grains by the transformation cycling. However, the misorientation within the austenite grains, characterized by the low angle grain boundaries and the kernel average misorientation (KAM) measured by EBSD, significantly changed by the transformation cycling. The starting material exhibited quite small internal distortions as shown in Fig. 5(a). After the first

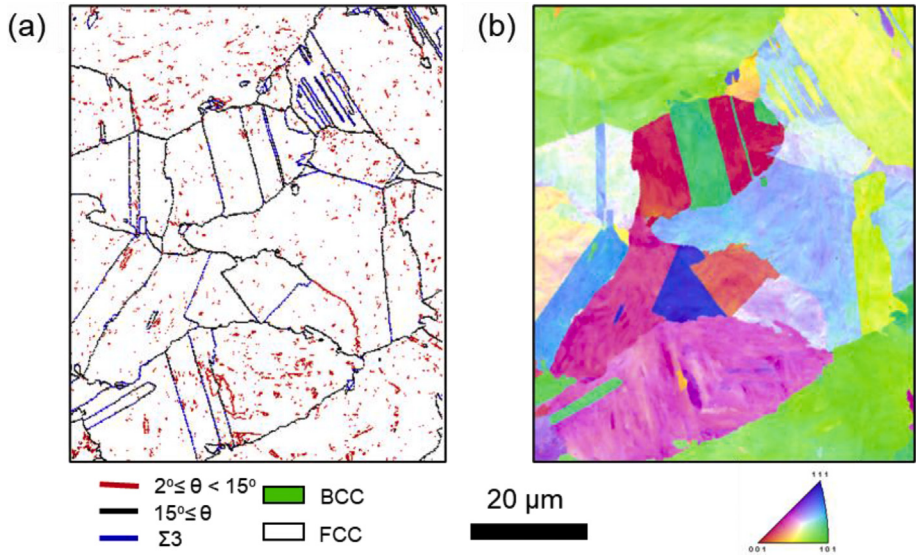

Fig. 4 – (a) Grain boundary map superimposed with phase map and (b) IPF map of the specimen after 1 cycle of martensitic transformation and reverse transformation treatment.

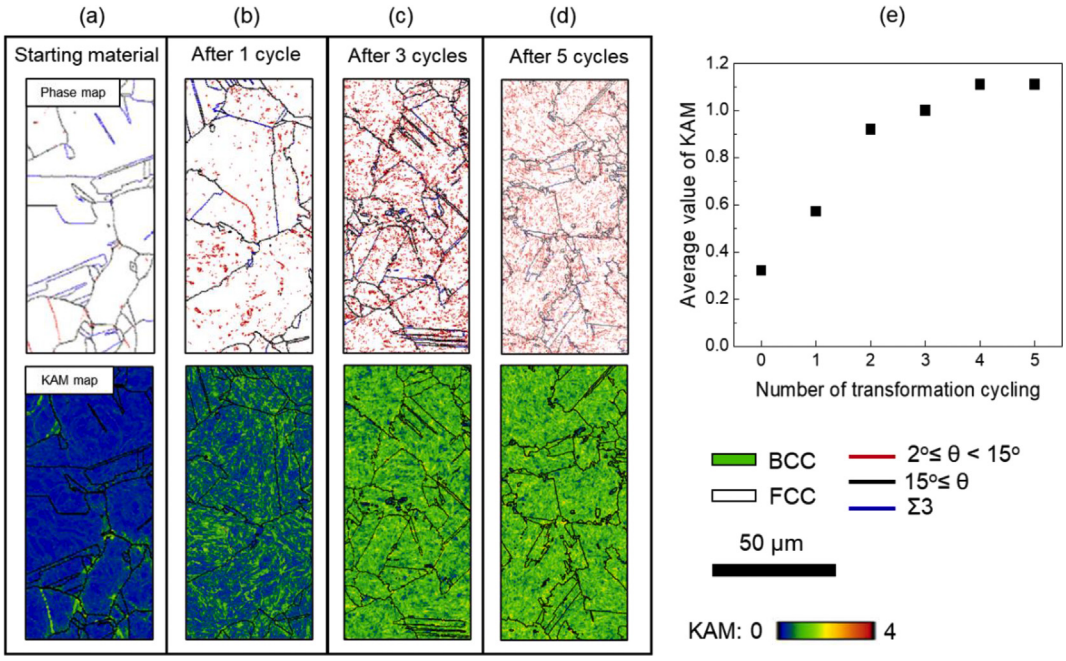

Fig. 5 – (a)–(d) Phase and grain boundary maps (upper) and KAM maps (lower) of the starting material and the specimens after 1, 3, and 5 cycles of the transformation cycling, respectively, in which the color scale from blue to red indicates the KAM value from 0 to 4; High angle grain boundaries are indicated by black solid lines. (e) Increase in the average KAM value of the specimen with increasing the number of the transformation cycling. The KAM is the average value of the misorientation between a center pixel with all the first nearest neighboring pixels in the EBSD mapping.

transformation cycling, the internal distortion within the austenite grains significantly increased. With further increasing the transformation cycling, the low angle grain boundaries within the austenite greatly increased and the KAM map of the specimen became mostly green or yellow, indicating that there was dramatic misorientation within the reversed austenite grains, as shown in Fig. 5 (c) and (d). Figure 5(e) shows that the average KAM value significantly increased from 0.32 to 0.57 b y 1 cycle of transformation cycling and further increased rapidly to 0.92 b y 2 cycles. After 2 cycles the average KAM value did not increase very much and it seemed to level off after 4 cycles. Figure 6(a) shows the XRD profiles of the starting material and the specimen after 5 cycles of the transformation cycling. It can be seen that the XRD profile of the reverse transformed specimen only consisted of the diffraction peaks of austenite, indicating a complete reverse transformation from martensite to austenite. This result was consistent with the EBSD observation shown in Fig. 4. In addition, it was noted that the diffraction peaks of the specimen broadened after the transformation cycling, as can be clearly observed in the inset in Fig. 6(a) in the case of the $(111)_\gamma$ peak. Such a diffraction peak broadening was caused by the non-uniform microstrain associated with the dislocations generated by the phase transformation by the transformation cycling. By using the Williamson-Hall method, the dislocation densities in the reversed austenite of the

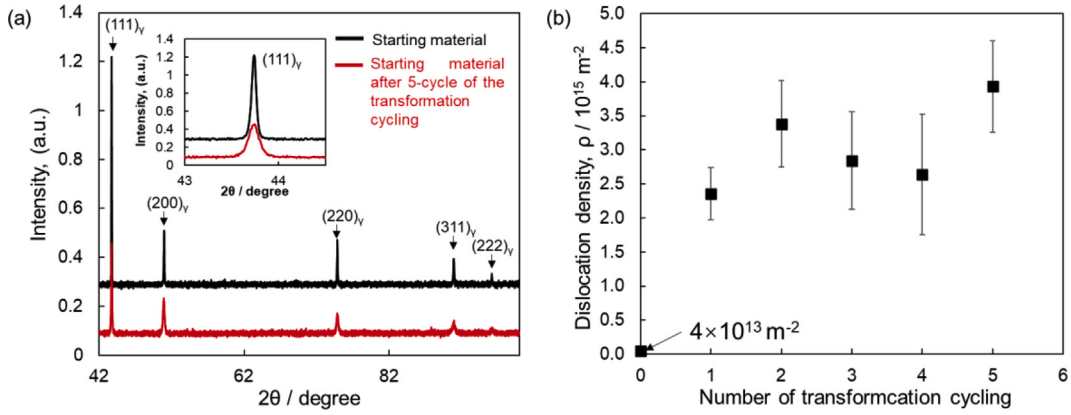

Fig. 6 – (a) XRD profiles of the starting material and the starting material after the 5-cycle of the transformation cycling. The embedded figure is the enlarged view of $(111)_\gamma$ peaks of the two profiles. (b) Dislocation density in the austenite as a function of the number of the transformation cycling.

specimens were calculated and plotted in Fig. 6(b). The dislocation density of the starting material is about 4×10^{13} m^{-2}, which is a typical value for a fully recrystallized microstructure [30]. After one transformation cycling, the dislocation density dramatically increased to 2.3×10^{15} m^{-2}. The dislocation density further increased to about 3×10^{15} m^{-2} after the second transformation cycling, and then it seemed to level off from the third cycle to the fifth cycle. These results are qualitatively in line with the changes of the average KAM value shown in Fig. 5(e).

It has been reported that the cycling of forward martensitic transformation and diffusional reverse transformation could be utilized to directly refine the microstructures of the steels without post deformation and annealing processes [31–33]. That is because the high density of lattice defects such as grain boundaries and dislocations in martensite can act as substantial nucleation sites for the diffusional reverse transformation to austenite, resulting in an effective grain refinement by the transformation cycling. However, the transformation cycling does not refine the grain size when the reverse transformation occurs in the non-diffusional type, because the non-diffusional reverse transformation leads to the identical austenite grain size to that before the transformation cycling, just as observed in Fig. 5 (a)–(c) in the present Fe-24Ni-0.3C steel. This was due to the so-called "austenite memory effect" [34] by that the reversed austenite reconstructed the structures of the original austenite. The austenite memory effect was possibly associated with the residual internal stress built up during the forward martensitic transformation, which can in turn assist the reverse transformation through the same pathway, but the mechanism has not been fully clarified yet.

Although the transformation cycling did not change the grain size of the reversed austenite, it significantly affected the deformation-induced martensitic transformation in the following cold rolling process. Figure 7 compares the XRD profiles of the 50% cold-rolled specimens with and without the transformation cycling prior to cold rolling. A great impact of the transformation cycling on the amount of deformation-induced martensite is noticed by the peak intensity. The calculation on the phase fraction revealed that about 70 vol% martensite formed in the transformation-cycling-treated specimen while only 15 vol% martensite was formed without prior transformation cycling. Generally, the stability of austenite can be enhanced by the repetition of martensitic transformation and its reverse shear transformation, since the austenite matrix is strengthened by the dislocations generated during transformation [35–37]. However, results in the present study clearly showed that the formation of deformation-induced martensite in Fe-24Ni-0.3C steel was promoted by the transformation cycling prior to deformation, suggesting that the austenite was destabilized, rather than stabilized, by the high density of dislocations introduced by the transformation cycling. To further confirm this, the austenite stability of the specimens with and without transformation cycling was evaluated by using DSC and the results are shown in Fig. 8. The heat flux in the DSC cooling curve indicated the occurrence of martensitic transformations which are exothermal reactions, and the M_s temperature was defined by the temperature at which the first flux starts to appear [38]. Despite that the M_s temperature was almost identical (about −25 °C) in both specimens, the specimen without transformation cycling showed one major peak followed by several distinct but smaller exothermal peaks when the temperature decreased from −25 °C to −80 °C, while the transformation-cycling-treated specimen showed a much more pronounced major exothermal peak that spanning from −25 °C to ~ −38 °C followed by several tiny peaks from −38 °C ~ −48 °C. These results indicated that the transformation kinetics upon cooling was dramatically enhanced due to the destabilizing of austenite by the transformation cycling.

Previously, Danilchenko et al. [39] investigated the effect of the cyclic $\gamma \leftrightarrow \alpha'$ transition on the thermal stability of an Fe-20.2%Ni-2.9%Mo-0.58%C alloy, and found that the formation of carbides in the reverse $\alpha' \rightarrow \gamma$ transformation reduced the stability of the austenite. However, this explanation might not apply to the present study. The TEM observation performed by Chen et al. [20] shows that in the Fe-24Ni-0.3C steel precipitate

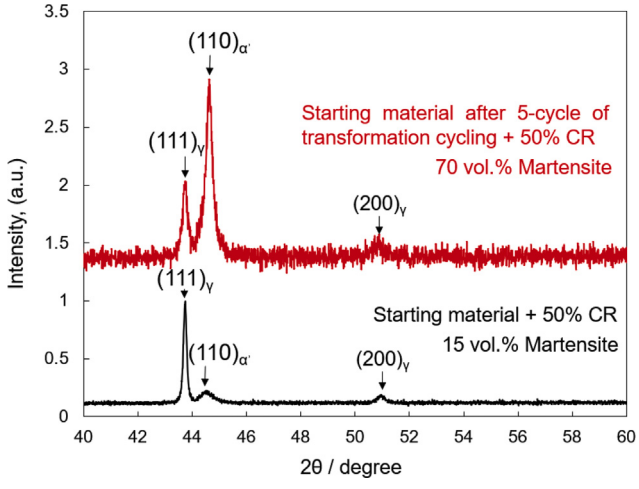

Fig. 7 – X-ray diffraction profiles of the 50% cold-rolled starting material with and without transformation cycling prior to cold rolling.

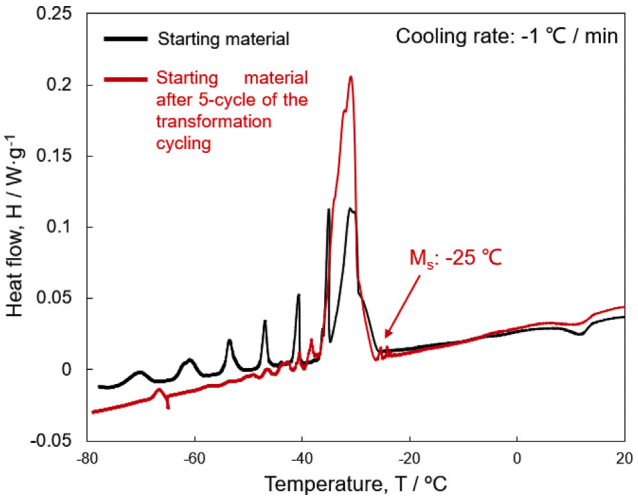

Fig. 8 – DSC cooling curves of the starting material and the transformation cycling treated starting material.

did not form when annealed at 530 °C for 600 s. In the present study the two annealing temperatures were both higher than 530 °C and the possibility of substantial precipitations of carbide can be excluded. As mentioned before, the stability of austenite could be increased by the strengthening of austenite due to dislocations. However, meanwhile, it is generally believed that dislocations in austenite act as favorable nucleation sites for the martensite and thus decrease the stability of austenite. It has been reported that the M_s temperature in Fe-Ni-C alloys increases by the austenite pre-strain [40–43]. Kajiwara et al. [43] found that even small pre-strain could significantly destabilize the austenite and increase the M_s temperature of the Fe-Ni and Fe-Ni-C alloys, and he proposed an alternative explanation that the dislocations introduced by the pre-strain can help to accommodate the transformation strain of martensite nucleation. Therefore, it is considered that in the present Fe-24Ni-0.3C steel the dislocations in austenite generated by the forward and reverse transformation were exactly the proper dislocations that can assist the austenite in plastically accommodating the transformation strain of the nucleating martensite and decrease the stability of austenite, although the nature of those dislocations remains to be investigated. On the other hand, as shown by Alaei et al. [29] the yield strength of the Fe-24Ni-0.3C steel was dramatically increased by the transformation cycling. It was considered that in the present study a higher mechanical driving force might have been acted on the transformation-cycling-treated specimen by the cold rolling, which may be another reason for the significant increase in the kinetics of martensitic transformation in the cold rolling.

After 50% cold rolling the specimen was annealed at 600 °C for 30 s, and the microstructures after annealing are shown in Fig. 9. The specimen fully consisted of austenite having partially recrystallized microstructures. The unrecrystallized region was characterized by the abundant deformation-induced low angle grain boundaries and the recrystallized region possessing equiaxed grains with a surprisingly small mean grain size of only 1.5 μm given that only 50% cold rolling was applied. Such a significant microstructures refinement by cold rolling and annealing was associated with the fact that the martensite introduced by the cold rolling lost its "austenite memory" because the internal stresses that had been generated by the transformation were completely perturbed by the applied plastic deformation [34]. As a result, upon annealing the martensite variants that had formed in one prior austenite grain transformed to austenite grains with different orientations, by which the original austenite grains were subdivided into much smaller grains [26,44]. Subsequently, recrystallization occurred in the reversed austenite having high dislocation densities and the mean grain size was further reduced to as small as 1.5 μm. Meanwhile, the deformed microstructures were maintained in the retained austenite since the driving force for recrystallization was much smaller than that of the reversed austenite [45].

After the first cold rolling and annealing, the material was subjected to a second cold rolling with a 90% thickness reduction and annealing process at 650 °C for 30 s. Figure 10(a) shows that the annealed specimen had fully austenitic microstructures consisting of equiaxed austenite grains with a measured grain size of 0.5 μm, and the corresponding size

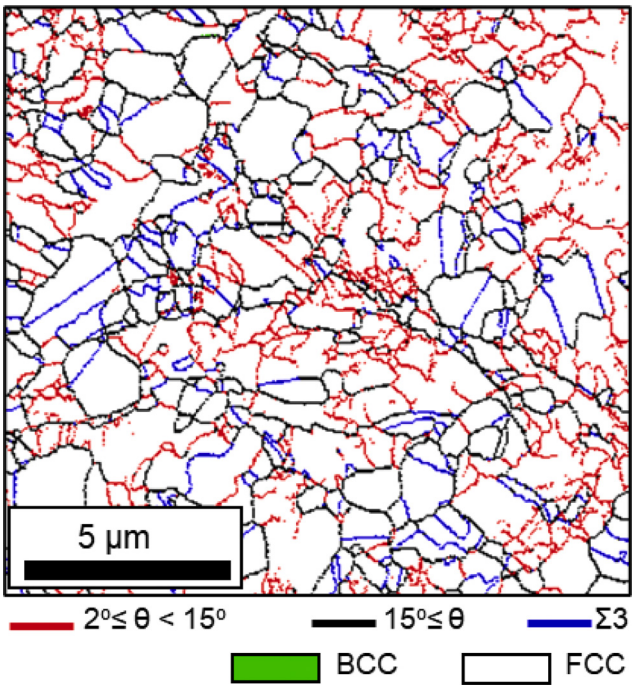

Fig. 9 – Grain boundary map superimposed with phase map of the 50% cold-rolled specimen after annealing at 600 °C for 30 s, observed in the transverse direction. The average misorientation of the specimen was 26.4°, in which the fraction of HAGB was 0.52 and that of annealing TB was 0.11.

distribution of austenite grains is shown in Fig. 10(b). Figure 10 (c) and (d) are the corresponding KAM map and the grain boundary misorientation distribution of the UFG specimen. The KAM map of the UFG specimen is mostly blue, indicating that the misorientation within austenite grains was quite small. Figure 10(d) shows that the UFG specimen had 87% HAGB and a fairly large fraction of annealing TB up to 0.23. The misorientation distribution had higher fractions in the regions of 5–26° and 50–60° compared with the Mackenzie distribution calculated for a random polycrystal [46], which might be attributed to the texture generated during the cold rolling [47]. These results clearly indicated that a fully recrystallized austenitic microstructure having submicrometer grain size was successfully fabricated. Two- or multiple-step cold rolling and annealing processes have been proposed for fabricating UFG metastable austenitic steels by utilizing the deformation-induced martensitic transformation and its reverse transformation to austenite upon subsequent annealing. Succeeded cases can be found in 301LN, 201, 304 stainless steels, and some Mn steels [16,17,48–50]. The first step cold rolling process usually results in mixed microstructures containing 50%–80% deformation-induced martensite and 20%–50% deformed austenite depending on the mechanical stability of the austenite. Upon the following annealing process, the reversion of deformation-induced martensite results in fine-grained austenite, while recrystallization takes place in the deformed austenite region that results in a relatively coarse austenite grain size [17,51]. Such bimodal microstructures of fine- and coarse-grained (CG) austenite could be

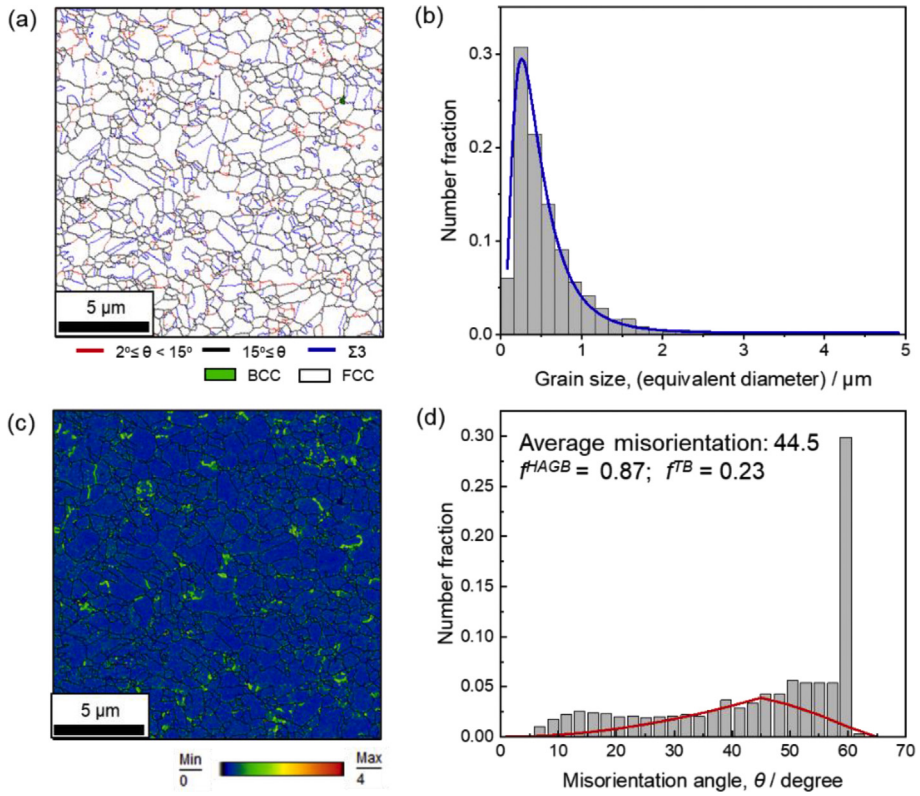

Fig. 10 – (a) Grain boundary map superimposed with phase map, (b) grain size distribution, (c) KAM map and (d) distribution of boundary misorientation of the finally obtained UFG specimen with a mean grain size of 0.5 μm, observed in the transverse direction of the cold-rolled plate. The blue curve in (b) is the fitted results by the lognormal function. The red curve in (d) indicates the MacKenzie distribution of misorientation angle in randomly oriented polycrystals.

further refined and homogenized by applying the second cold-rolling and annealing processes in which the mechanically less stable coarse austenitic microstructures are refined again through deformation-induced martensitic transformation and reverse transformation [52]. It should be emphasized that the feasibility of achieving relatively homogeneous UFG microstructures by these processes vitally relies on the stability of the austenite, since high densities of crystalline defects in deformation-induced martensite provide substantial nucleation sites for achieving fine-grained reversed austenite. Therefore, direct two-step or multiple-step cold rolling and annealing process inoperative for fabricating UFG Fe-24Ni-0.3C steel, since austenite in Fe-24Ni-0.3C steel has high stability against martensitic transformation during cold rolling due to the high content of austenite stabilizing elements such as nickel and carbon. In fact, in the authors' previous study the smallest grain size in Fe-24Ni-0.3C steel was limited to 1.3 μm by two-step cold rolling and annealing [21] due to the lack of the formation of deformation-induced martensite during cold rolling. In the present study, the prior transformation cycling greatly accelerated the deformation-induced martensitic transformation during the subsequent deformation and enhanced grain refinement efficiency, resulting in the formation of the fine-grained microstructure after the first cold rolling and annealing. The second cold rolling and annealing made the microstructure further refined to the UFG scale and more homogeneous.

The tensile stress-strain curves of the UFG specimen and a CG specimen (d_{ave} = 35 μm) are shown in Fig. 11(a). The CG specimen shows a low yield strength of about 180 MPa, an ultimate tensile strength of 1050 MPa, and large uniform elongation of 70%. By contrast, the UFG specimen exhibited a significantly higher yield strength of 680 MPa which is 3.7 times higher than that of the CG specimen, due to the significant grain size refinement strengthening. Surprisingly, a large uniform elongation of 70% was maintained in the UFG specimen which was almost the same as that of the CG specimen. These results indicated an overcoming of the strength-ductility trade-off in the Fe-24Ni-0.3C steel by effective grain refinement realized by the processes in the present study. Such an excellent combination of tensile strength and elongation of the CG and the UFG specimens were ascribed to the extra strain hardening caused by the formation of deformation-induced martensite during tensile deformation. Figure 11 (b) shows the strain hardening rate curves and the true stress-strain curves of the CG and the UFG specimens. The volume fraction of martensite in the UFG specimen at different strain stages obtained by SEM-EBSD measurement is superimposed in Fig. 11(b), in which that of the CG specimen shown in Ref. [21] is also plotted. Due to the formation of the martensite, a significant increase in the strain hardening rate was observed in both two specimens in the plastic region, which postponed the onset of the necking in the tensile deformation and thus resulted in the large uniform elongation as well as the high

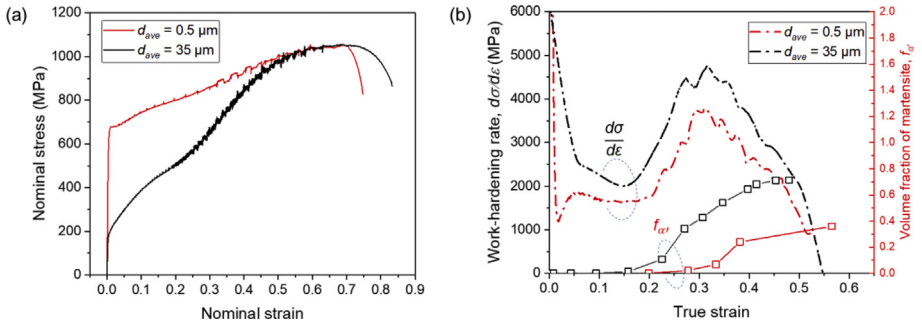

Fig. 11 – (a) Nominal stress-strain curves and (b) corresponding strain hardening rate curves and evolution of the volume fraction of martensite during the tensile deformation in the UFG specimen (d_{ave} = 0.5 μm) and CG specimen (d_{ave} = 35 μm). Since the stress-strain curves have severe serrations, the strain hardening rate curves in (b) were obtained from smoothing processed true stress-strain curves, which only roughly represent the tendency of strain hardening.

tensile strength. It can be seen that as the austenite grain size decreased, the initiation of the deformation-induced martensitic transformation was delayed to a later strain stage and its formation with the strain was greatly suppressed. After tensile failure, 71% austenite transformed to martensite in the CG specimen while that in the UFG specimen was only 36%. It was interesting that the increment in the strain hardening rate caused by the martensite formation in the UFG specimen did not decrease so much compared with that in the CG specimen, even though the kinetics of deformation-induced martensitic transformation was greatly suppressed by the grain refinement. This might be the reason why the UFG specimen could overcome the strength-ductility-trade-off relationship. However, details of the deformation mechanisms of the UFG specimen are still unclear at present, which will be investigated in further studies.

4. Summary

In the present study, a UFG Fe-24Ni-0.3C specimen with a mean grain size of 0.5 μm was successfully fabricated by a two-step cold rolling and annealing process. Prior to the first cold rolling, the material was subjected to 5 cycles of cryogenic treatment and annealing treatment, which was a crucial step for the ultra-grain refinement in the process. During the cyclic treatment, the martensitic transformation and its reverse transformation to austenite repeatedly occurred. The transformation cycling introduced high dislocation densities that remained in the reversed austenite. The high dislocation density greatly decreased the stability of austenite and enhanced the kinetics of the deformation-induced martensitic transformation in the following cold rolling process. The substantial amount of deformation-induced martensite significantly promoted the efficiency of the grain refinement in the process. A fine-grained microstructure with a mean grain size of 1.5 μm in the recrystallized region was realized by only 50% cold rolling with subsequent annealing. After the second step of cold rolling and annealing, a fully recrystallized UFG austenitic specimen with a mean grain size of 0.5 μm was obtained. The UFG specimen exhibited an excellent balance of strength and ductility, which was contributed to the combination of UFG structure and TRIP effect.

Declaration of Competing Interest

The authors declare that they have no known competing financial interests or personal relationships that could have appeared to influence the work reported in this paper.

Acknowledgment

The present study was financially supported by the Elements Strategy Initiative for Structural Materials (ESISM, No. JPMXP0112101000), JST CREST (JPMJCR1994), and JSPS (Japan Society for the Promotion of Science) KAKENHI (Nos. 15H05767, 20H00306) all through the Ministry of Education, Culture, Sports, Science and Technology (MEXT), Japan. W.M was financially supported by China Scholarship Council (CSC), China for his PhD course. All of the supports are gratefully appreciated.

REFERENCES

[1] Tsuji N, Ito Y, Saito Y, Minamino Y. Strength and ductility of ultrafine grained aluminum and iron produced by ARB and annealing. Scripta Mater 2002;47:893–9. https://doi.org/10.1016/S1359-6462(02)00282-8.

[2] Jafarian H. Characteristics of nano/ultrafine-grained austenitic TRIP steel fabricated by accumulative roll bonding and subsequent annealing. Mater Char 2016;114:88–96. https://doi.org/10.1016/j.matchar.2016.02.012.

[3] Misra RDK, Nayak S, Mali SA, Shah JS, Somani MC, Karjalainen LP. Microstructure and deformation behavior of phase-reversion-induced nanograined/ultrafine-grained austenitic stainless steel. Metall. Mater. Trans. A Phys. Metall. Mater. Sci. 2009;40:2498–509. https://doi.org/10.1007/s11661-009-9920-3.

[4] Tamura I. Deformation-induced martensitic transformation and transformation-induced plasticity in steels. Met Sci 1982;16:245–53. https://doi.org/10.1179/030634582790427316.

[5] Jacques PJ. Transformation-induced plasticity for high strength formable steels. Curr Opin Solid State Mater Sci 2004;8:259–65. https://doi.org/10.1016/j.cossms.2004.09.006.

[6] Zhilyaev AP, Langdon TG. Using high-pressure torsion for metal processing: fundamentals and applications. Prog Mater Sci 2008;53:893–979. https://doi.org/10.1016/j.pmatsci.2008.03.002.

[7] Saito Y, Utsunomiya H, Tsuji N, Sakai T. Novel ultra-high straining process for bulk materials—development of the accumulative roll-bonding (ARB) process. Acta Mater 1999;47:579–83. https://doi.org/10.1016/S1359-6454(98)00365-6.
[8] Tsuji N, Saito Y, Utsunomiya H, Tanigawa S. Ultra-fine grained bulk steel produced by accumulative roll-bonding (ARB) process. Scripta Mater 1999;40:795–800. https://doi.org/10.1016/S1359-6462(99)00015-9.
[9] Valiev RZ, Langdon TG. Principles of equal-channel angular pressing as a processing tool for grain refinement. Prog Mater Sci 2006;51:881–981. https://doi.org/10.1016/j.pmatsci.2006.02.003.
[10] Tomimura K, Takaki S, Tanimoto S, Tokunaga Y. Optimal chemical composition in Fe-Cr-Ni alloys for ultra grain refining by reversion from deformation induced martensite. ISIJ Int 1991;31:721–7. https://doi.org/10.2355/isijinternational.31.721.
[11] Järvenpää A, Jaskari M, Kisko A, Karjalainen P. Processing and properties of reversion-treated austenitic stainless steels. Metals 2020;10. https://doi.org/10.3390/met10020281.
[12] Sohrabi MJ, Naghizadeh M, Mirzadeh H. Deformation-induced martensite in austenitic stainless steels: a review. Arch. Civ. Mech. Eng. 2020;20:1–24. https://doi.org/10.1007/s43452-020-00130-1.
[13] Odnobokova M, Belyakov A, Enikeev N, Molodov D, Kaibyshev R. Annealing behavior of a 304L stainless steel processed by large strain cold and warm rolling. Materials Science and Engineering A 2017;689(October 2016):370–83. https://doi.org/10.1016/j.msea.2017.02.073.
[14] Gao S, Bai Y, Zheng R, Tian Y, Mao W, Shibat A, et al. Mechanism of huge Lüders-type deformation in ultrafine grained austenitic stainless steel. Script Mater 2019;159:28–32. https://doi.org/10.1016/j.scriptamat.2018.09.007.
[15] Xu D, Li G, Wan X, Xiong R, Xu G, Wu KM, et al. Deformation behavior of high yield strength – High ductility ultrafine-grained 316LN austenitic stainless steel. Materials Science and Engineering: A 2017;688:407–15. https://doi.org/10.1016/j.msea.2017.02.009.
[16] Moallemi M, Kermanpur A, Najafizadeh A, Rezaee A, Samaei Baghbadorani H. Formation of nano/ultrafine grain structure in a 201 stainless steel through the repetitive martensite thermomechanical treatment. Mater Lett 2012;89:22–4. https://doi.org/10.1016/j.matlet.2012.08.058.
[17] Niu G, Wu H, Zhang D, Gong N, Tang D. Heterogeneous nano/ultrafine-grained medium Mn austenitic stainless steel with high strength and ductility. Mater Sci Eng 2018;725:187–95. https://doi.org/10.1016/j.msea.2018.04.022.
[18] Ishida K, Nishizawa T. Ferrite/Austenite stabilizing parameter of alloying elements in steel at 200~500°C. Trans. Japan Inst. Met. 1974;15:217–24. https://doi.org/10.2320/matertrans1960.15.217.
[19] Chen S, Shibata A, Zhao LJ, Gao S, Tian YZ, Tsuji N. Microstructural evolution of metastable austenitic steel during high-pressure torsion and subsequent heat treatment. IOP Conf Ser Mater Sci Eng 2014;63:012053. https://doi.org/10.1088/1757-899X/63/1/012053.
[20] Chen S, Shibata A, Gao S, Tsuji N. Formation of fully annealed nanocrystalline austenite in FeNiC alloy. Mater Trans 2014;55:223–6. https://doi.org/10.2320/matertrans.M2013324.
[21] Mao WQ, Gao S, Gong W, Park MH, Bai Y, Shibata A, et al. Influence of grain size on work-hardening behavior of Fe-24Ni-0.3C metastable austenitic steel. In: Proceedings of the international conference on martensitic transformations; 2018. p. 95–8. https://doi.org/10.1007/978-3-319-76968-4_15. Chicago.
[22] De AK, Murdock DC, Mataya MC, Speer JG, Matlock DK. Quantitative measurement of deformation-induced martensite in 304 stainless steel by X-ray diffraction. Scripta Mater 2004;50:1445–9. https://doi.org/10.1016/j.scriptamat.2004.03.011.
[23] Williamson GK, Hall WH. X-ray line broadening from filed aluminium and wolfram. Acta Metall 1953;1:22–31. https://doi.org/10.1016/0001-6160(53)90006-6.
[24] Williamson GK, Smallman III RE. Dislocation densities in some annealed and cold-worked metals from measurements on the X-ray Debye-Scherrer spectrum. Philos Mag 1956;1:34–46. https://doi.org/10.1080/14786435608238074.
[25] Pan B, Qian K, Xie H, Asundi A. Two-dimensional digital image correlation for in-plane displacement and strain measurement: a review. Meas Sci Technol 2009;20:062001. https://doi.org/10.1088/0957-0233/20/6/062001.
[26] Tomimura K, Takaki S, Tokunaga Y. Reversion mechanism from deformation induced martensite to austenite in metastable austenitic stainless steels. ISIJ Int 1991;31:1431–7. https://doi.org/10.2355/isijinternational.31.1431.
[27] Krauss G. Fine structure of austenite produced by the reverse martensitic transformation. Acta Metall 1963;11:499–509. https://doi.org/10.1016/0001-6160(63)90085-3.
[28] Nakada N. Direct observation of martensitic reversion from lenticular martensite to austenite in Fe-Ni alloy. Mater Lett 2017;187:166–9. https://doi.org/10.1016/j.matlet.2016.10.056.
[29] Alaei A, Jafarian H, Eivani AR. Observation austenite memory and significant enhancement of tensile properties during cyclic reverse martensite transformation in a Fe-Ni-C TRIP steel. Mater Sci Eng 2016;676:342–50. https://doi.org/10.1016/j.msea.2016.09.003.
[30] Shintani T, Murata Y. Evaluation of the dislocation density and dislocation character in cold rolled Type 304 steel determined by profile analysis of X-ray diffraction. Acta Mater 2011;59:4314–22. https://doi.org/10.1016/j.actamat.2011.03.055.
[31] Park MH, Shibata A, Tsuji N. Grain refinement of 2Mn-0.1C steel by repetitive heat treatment and recrystallization. IOP Conf Ser Mater Sci Eng 2015;89. https://doi.org/10.1088/1757-899X/89/1/012041.
[32] Shibata A, Daido S, Terada D, Tsuji N. Microstructures of pearlite and martensite transformed from ultrafine-grained austenite fabricated through cyclic heat treatment in medium carbon steels. Mater Trans 2013;54:1570–4. https://doi.org/10.2320/matertrans.MH201312.
[33] Chiba T, Hassan S, Miyamoto G, Furuhara T. Grain refinement by cyclic displacive forward/reverse transformation in Fe-High-Ni alloys. Metall. Mater. Trans. A Phys. Metall. Mater. Sci. 2017;48:1–7. https://doi.org/10.1007/s11661-017-4152-4.
[34] Nakada N, Tsuchiyama T, Takaki S, Hashizume S. Variant selection of reversed austenite in lath martensite. ISIJ Int 2007;47:1527–32. https://doi.org/10.2355/isijinternational.47.1527.
[35] Tomota Y, Maki T. Effect of transformation cycling on the ε martensitic transformation in Fe-Mn alloys. ISIJ Int 1990;30:666–73. https://doi.org/10.2355/isijinternational.30.666.
[36] Edmondson B, Ko T. Spontaneous deformation of austenite during martensitic transformations. Acta Metall 1954;2:235–41. https://doi.org/10.1016/0001-6160(54)90164-9.
[37] Imai Y, Izumiyama M, Hanada S. Effect of cyclic heat treatment on the martensitic transformation in the Iron-Nickel binary alloys. J. Japan Inst. Met. Mater. 1967;31:898.
[38] Hayzelden C, Cantor B. The martensite transformation in FeNiC alloys. Acta Metall 1986;34:233–42. https://doi.org/10.1016/0001-6160(86)90194-X.
[39] Danilchenko VE, Nedolya AV. Austenite stabilization of Fe-Ni alloy. Acta Phys Pol 1994;86:617–20. https://doi.org/10.12693/aphyspola.86.617.

[40] Wollmann DR, Guimarães JRC. The effects of plastic deformation and thermal stabilization of austenite upon martensite burst kinetics. Scripta Metall 1973;7:355–9. https://doi.org/10.1016/0036-9748(73)90055-0.
[41] Guimarães JRC, Gomes JC. The effects of pre-deformation and temperature of the transformation-deformation behavior of Fe-31%Ni-0.1%C. Mater Sci Eng 1979;39:187–91. https://doi.org/10.1016/0025-5416(79)90058-2.
[42] Tokizane M. The effect of tensile pre-straining on nucleation of martensite in an Fe-Ni-C alloy. Scripta Metall 1976;10:459–62. https://doi.org/10.1016/0036-9748(76)90173-3.
[43] Kajiwara S. Roles of dislocations and grain boundaries in martensite nucleation. Metall Mater Trans A 1986;17:1693–702. https://doi.org/10.1007/BF02817268.
[44] Misra RDK, Nayak S, Venkatasurya PKC, Ramuni V, Somani MC, Karjalainen LP. Nanograined/ultrafine-grained structure and tensile deformation behavior of shear phase reversion-induced 301 austenitic stainless steel. Metall. Mater. Trans. A Phys. Metall. Mater. Sci. 2010;41:2162–74. https://doi.org/10.1007/s11661-010-0230-6.
[45] Kisko A, Hamada AS, Talonen J, Porter D, Karjalainen LP. Effects of reversion and recrystallization on microstructure and mechanical properties of Nb-alloyed low-Ni high-Mn austenitic stainless steels. Mater Sci Eng 2016;657:359–70. https://doi.org/10.1016/j.msea.2016.01.093.
[46] Mackenzie JK, Thomson MJ. Some statistics associated with the random disorientation of cubes. Biometrika 1957;44:205. https://doi.org/10.2307/2333253.
[47] Mason JK, Schuh CA. The generalized Mackenzie distribution: disorientation angle distributions for arbitrary textures. Acta Mater 2009;57:4186–97. https://doi.org/10.1016/j.actamat.2009.05.016.
[48] Sun GS, Du LX, Hu J, Xie H, Wu HY, Misra RDK. Ultrahigh strength nano/ultrafine-grained 304 stainless steel through three-stage cold rolling and annealing treatment. Mater Char 2015;110:228–35. https://doi.org/10.1016/j.matchar.2015.11.001.
[49] Sun GS, Du LX, Hu J, Misra RDK. Microstructural evolution and recrystallization behavior of cold rolled austenitic stainless steel with dual phase microstructure during isothermal annealing. Mater Sci Eng 2018;709:254–64. https://doi.org/10.1016/j.msea.2017.10.054.
[50] Järvenpää A, Jaskari M, Man J, Karjalainen LP. Austenite stability in reversion-treated structures of a 301LN steel under tensile loading. Mater Char 2017;127:12–26. https://doi.org/10.1016/j.matchar.2017.01.040.
[51] Ravi Kumar B, Sharma S. Recrystallization behavior of a heavily deformed austenitic stainless steel during iterative type annealing. Metall. Mater. Trans. A Phys. Metall. Mater. Sci. 2014;45:6027–38. https://doi.org/10.1007/s11661-014-2543-3.
[52] Lee CY, Yoo CS, Kermanpur A, Lee YK. The effects of multi-cyclic thermo-mechanical treatment on the grain refinement and tensile properties of a metastable austenitic steel. J Alloys Compd 2014;583:357–60. https://doi.org/10.1016/j.jallcom.2013.08.161.